Molecular dynamics study on thermal dehydration process of epsomite (MgSO4.7H2O)

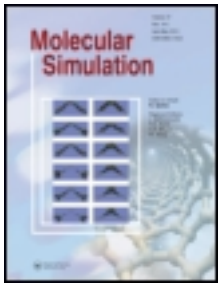

Molecular Simulation
Publication details, including instructions for authors and subscription information:
http://www.tandfonline.com/loi/gmos20

Molecular dynamics study on thermal dehydration process of epsomite ($MgSO_4 \cdot 7H_2O$)

Huaichen Zhang[a], Eldhose Iype[a], Silvia V. Nedea[a] & Camilo C.M. Rindt[a]
[a] Department of Mechanical Engineering, Eindhoven University of Technology, Den Dolech 2, 5612AZ, Eindhoven, The Netherlands
Published online: 11 Dec 2013.

To cite this article: Huaichen Zhang, Eldhose Iype, Silvia V. Nedea & Camilo C.M. Rindt , Molecular Simulation (2013): Molecular dynamics study on thermal dehydration process of epsomite ($MgSO_4 \cdot 7H_2O$), Molecular Simulation, DOI: 10.1080/08927022.2013.854891

To link to this article: http://dx.doi.org/10.1080/08927022.2013.854891

Molecular Simulation, 2013
http://dx.doi.org/10.1080/08927022.2013.854891

Taylor & Francis
Taylor & Francis Group

Molecular dynamics study on thermal dehydration process of epsomite ($MgSO_4 \cdot 7H_2O$)

Huaichen Zhang, Eldhose Iype, Silvia V. Nedea and Camilo C.M. Rindt*

Department of Mechanical Engineering, Eindhoven University of Technology, Den Dolech 2, 5612AZ Eindhoven, The Netherlands

(*Received 14 June 2013; final version received 8 October 2013*)

Water vapour sorption in salt hydrates is one of the most promising means of compact, low loss and long-term solar heat storage in the built environment. Among all, epsomite ($MgSO_4 \cdot 7H_2O$) excels for its high-energy storage density and vast availability. However, in practical applications, the slow kinetics and evident structural changes during hydration and dehydration significantly jeopardise the heat storage/recovery rate. A molecular dynamics (MD) study is carried out to investigate the thermal properties and structural changes in the thermal dehydration process of the epsomite. The MD simulation is carried out at 450 K and a vapour pressure of 20 mbar, in accordance with experimental heat storage conditions. The study identifies the dehydration as multiple stages from the initial quick water loss and collapse of the crystal framework to the adsorption of water molecules, which inhibits complete dehydration. Further, the anisotropic diffusion behaviour supports the important role of the porous matrix structure in the heat and mass transfer process. The enthalpy changes, partial densities, mass diffusion coefficients of water and radial distribution functions are calculated and compared with corresponding experimental data to support the conclusions.

Keywords: molecular dynamics simulation; diffusion coefficient; magnesium sulphate; thermal dehydration

1. Introduction

Compact heat storage is widely used in various applications. For example, in seasonal heat storage systems, the energy consumption in the built environment in winter can be cut down by recovering the solar heat stored in the summer. Recent studies suggested using salt hydrates as long-term thermo-chemical heat storage materials for their high storage capacity, low environmental impact and low heat loss.[1] In summer, dry hot air from solar collectors is blown into the reactor to dry up the hydrates to charge the storage tank; in winter, humid air is absorbed by anhydrous salts to extract heat from the storage tank. A recent study identified epsomite ($MgSO_4 \cdot 7H_2O$) as one of the most promising thermo-chemical heat storage materials,[2] and subsequent studies were carried out to improve its thermal properties.[3] Epsomite is cost-effective, non-toxic, non-corrosive and has a large storage capacity of 2.8 GJ/m^3 when fully dehydrated. Preliminary measurements showed that sensible heat losses only comprise about 10% of the total energy stored. However, in applications, clotting and expansion during hydration and formation of powdery particles during dehydration can block the air flow or reduce the effective area of adsorption; melting of the heptahydrate during dehydration may reduce the connectivity of the pores, change the internal surface structure and block the air flow through the reactor. These practical issues increase the difficulty in the reactor design, which relies on a detailed understanding of the vapour transport by diffusion and convection.

The thermal dehydration process of epsomite was extensively studied by experiments. One crucial step is the opening of wider channels and cracks, which allows the transportation of water molecules, while the formation of cracks is then influenced by the rate of dehydration and the growth of superficial textures.[4] The dehydration rate and pathways are further dependent on the water vapour pressure.[5,6] The structural changes during dehydration are identified and possible metastable states at different temperatures and vapour pressures are characterised.[7–10] These give better understandings and predictions about the dehydration process at larger scales. Van Essen et al. [2] measured the heat flux during dehydration at 23 mbar vapour pressure according to experimental heat storage conditions, which laid the foundation and brought our interest to the present work. However, the vapour transport process, especially on powder/grain scale, is still unclear, and at these small scales, detailed local properties such as diffusion coefficients remain difficult to be directly studied through experiments. A molecular-scale investigation into the dehydration process seems necessary in order to unveil these details and to identify the factors that affect the diffusion through the surface layers. Iype et al. [11] quantified the energies of distinct magnesium sulphate hydrates [11] and identified various hydrogen-bonding networks [12] from density functional theory (DFT) calculations. These calculations show that there is no

*Corresponding author. Email: c.c.m.rindt@tue.nl

significant charge transfer during the dehydration process, which opened up the possibility of performing a large-scale non-reactive molecular dynamics (MD) simulation. MD techniques were used to study the dehydration from other inorganic crystalline structures [13,14]; however, such techniques have not been applied to epsomite yet.

In this study, we present the results of MD simulations on the dehydration of epsomite at 450 K (177°C) and approximately 20 mbar of water vapour pressure. We report various thermodynamic properties including energy, partial densities, radial distribution functions (RDFs) and diffusion coefficients. The dehydration process and the water transport by diffusion are investigated based on molecular observations as well as on quantitative analyses.

2. Methodology

2.1 *Molecular dynamics*

Computer simulations, and in particular non-equilibrium molecular dynamics methods based on non-equilibrium thermodynamics (NET), offer a valuable tool for the study of transport properties of materials. One key assumption of the NET theory is that any small element of a system can be considered to be in a state of local equilibrium.[15] This enables the calculation of dynamic properties in non-equilibrium states. In this study, a general-purpose GROMOS53A6 force field [16] additionally optimised for hydration and solvation was selected in the energy minimisation and MD simulations. Simple point charge (SPC) water model [17] was adopted because of its good approximation in liquid–vapour coexistence.[18] The total potential energy in the molecular model is

$$E_{\text{pot}} = \sum_{\text{bonds}} \frac{1}{4} k_{\text{bond},ij}\left(r_{ij}^2 - r_{0,ij}^2\right)^2 + \sum_{\text{angles}} \frac{1}{2} k_{\text{angle},ijk}(\cos\theta_{ijk} - \cos\theta_{0,ijk})^2 + \sum_{\text{non-bonded} r_{ij} < r_{\text{c,LJ}}} \left(\frac{A_{ij}}{r_{ij}^{12}} - \frac{B_{ij}}{r_{ij}^{6}}\right) + \sum_{\text{non-bonded} r_{ij} < r_{\text{c,E}}} f \frac{\text{erfc}(\beta r_{ij})}{r_{ij}} q_i q_j + E_{\text{long-range}}, \quad (1)$$

where the first three terms represent the S—O bond energy in the sulphate dianion, the O—S—O bond angle energy in the sulphate dianion and the non-bonded Lennard-Jones potential within the cut-off radius, respectively. The last two terms are for the electrostatic interactions within the cut-off radius and the long-range corrections using the smoothed particle mesh Ewald (PME) summation method. [19]

2.2 *Simulation details*

To simulate the dehydration of $MgSO_4{\cdot}7H_2O$ from a perfect crystalline surface, we took the crystalline structure from a neutron diffraction study [20] at 2 K. A cuboid simulation box consisting of $5 \times 5 \times 6$ cells, each of which contained 4 Mg^{2+} dications, 4 SO_4^{2-} dianions and 28 H_2O molecules, was constructed with periodic boundary conditions in all directions, and was equilibrated under 1 bar and 450 K using a Berendsen barostat and thermostat [21] for a sufficient time of 500 ps. This was to prevent thermal expansion in the later constant NVT simulation. After equilibration, the crystal was cleaved at the (001) surfaces. The cleaved crystal slab had $5 \times 5 \times 3$ cells, which summed up to 300 Mg^{2+}, 300 SO_4^{2-} and 2100 H_2O entities. The 2.036 nm thick slab was then attached to two vacuum spaces of 50 nm in thickness, as illustrated in Figure 1. We first applied a steepest descent energy minimisation on this newly generated configuration before the MD simulation was started.

GROMACS4.5.4 [22] was used to carry out the MD simulation. Short-range electrostatic interactions and van der Waals interactions were cut off at 2.5 nm. Long-range electrostatic interactions were calculated using PME [19] with $20 \times 20 \times 340$-sized meshes. A correction term was added in z-direction to produce a pseudo 2D summation, in prevention of slab–slab interactions.[22] Initial velocities of the particles were generated according to a Boltzmann distribution at 450 K. In this simulation, the temperature was

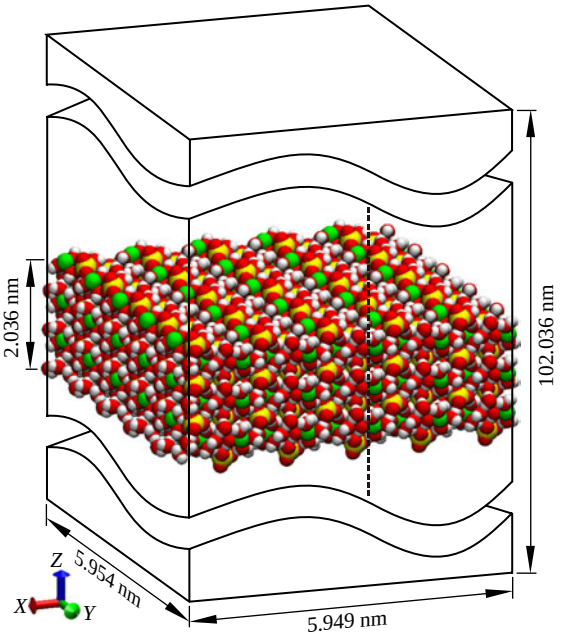

Figure 1. (Colour online) The periodic simulation cuboid contains a crystal slab cleaved at the (001) surfaces and two vacuum spaces attached onto both sides of the crystal.

kept at 450 K using a Berendsen thermostat with a time constant $\tau_t = 0.1$ ps. The constant temperature simulation ensures a correct energy calculation. After 300 ns of simulation time, the temperature was instantly raised to 600 K for another 25 ns, and then raised to 800 K for the final 75 ns, to completely dehydrate the crystal.

Water molecules in the slab-vacuum system were labelled as 'free' if they are at least 1 nm away from the crystal slab surface or 'confined' if otherwise. Note that assuming the ideal gas law, a single water molecule in the vacuum space will result in 17.4 mbar of vapour pressure, leading to high fluctuations in pressure. For every 100 ps, all free water molecules but the nearest one from the slab surface were removed from the system. This time interval is sufficient, as a preliminary simulation has shown that a faster removal did not speed up the dehydration process. The aforementioned removal scheme keeps an approximate vapour pressure of 20 mbar.

2.3 *Data analysis*

The diffusion of water is one of the factors that govern the water transport in the dehydration process, which is of special interest in continuum-scale models. Local diffusion constants can be easily calculated through velocity autocorrelation functions (VACFs) by Green–Kubo relation. Theories, simulations and experiments have proved that VACFs decay as $t^{-3/2}$,[23] indicating a fast convergence of the calculation. However, Allen and Tildesley [24] pointed out that the long-time contribution could not be ignored.[24] It should also be noted that because of the slow diffusion kinetics in the crystal slab, the time constant of the decay is relatively large, and hence, the integral requires much more data to get convergence, leaving it less computationally competitive than the mean-squared displacement (MSD) fitting method by Einstein relations. The MSD fitting method is in essence an integral of the Green–Kubo relation, and therefore, the atomic vibrations in the solid can be cancelled out, and consequently fewer frames are needed for calculating the ensemble average. The local diffusion coefficients are calculated numerically by the following equations:

$$D_{xyz} = \frac{1}{6(t - t_0)} \sum_{i \in \mathrm{A}, \mathbf{r}_i \in \Omega} \|\mathbf{r}_i(t) - \mathbf{r}_i(t_0)\|^2 \tag{2}$$

$$D_z = \frac{1}{2(t - t_0)} \sum_{i \in \mathrm{A}, \mathbf{r}_i \in \Omega} \|[\mathbf{r}_i(t) - \mathbf{r}_i(t_0)] \cdot \mathbf{n}_z\|^2, \tag{3}$$

where $\mathbf{r}_i$ is the position of atom i, i represents all atoms belonging to chemical species A, Ω is a local region, t is the time, t_0 is the time level at which a molecule enters the local region, $\mathbf{n}_z = [0\,0\,1]^{\mathrm{T}}$ is the unit vector in z-direction, D_{xyz} is the 3D diffusion coefficient and D_z is the z component of the diffusion coefficient. Note that usually t should be much larger than it t_0 to ensure a correct result since the MSDs show an asymptotic behaviour. In our work, the diffusion coefficients were obtained by fitting the linear region of MSDs over time, which no longer requires a large $(t - t_0)$.

Local partial densities are uniform in x and y directions in early dehydration stages. Therefore, the partial densities as functions of z give very useful information on the dehydration behaviours. The local partial density is calculated as:

$$\rho_{\mathrm{A}} = \frac{1}{(t_1 - t_0)V_\Omega} \int_{t_0}^{t_1} \sum_{i \in \mathrm{A}, \mathbf{r}_i \in \Omega} m_i \, \mathrm{d}t, \tag{4}$$

where V is the volume of the local region and m is the mass.

RDFs provide information on the structural changes and are calculated as:

$$g_{\mathrm{AB}}(r) = \frac{\langle \rho_{\mathrm{B}}(r) \rangle}{\langle \rho_{\mathrm{B}} \rangle_{\mathrm{local}}} = C \frac{1}{t_1 - t_0} \int_{t_0}^{t_1} \frac{1}{N_{\mathrm{A}}(t)} \sum_{i \in \mathrm{A}} \sum_{j \in \mathrm{B}} \frac{\delta(r_{ij}(t) - r)}{4\pi r^2} \, \mathrm{d}t \tag{5}$$

$$C = \frac{\langle \rho_{\mathrm{B}} \rangle_{\mathrm{global}}}{\langle \rho_{\mathrm{B}} \rangle_{\mathrm{local}}} = \frac{\langle V_{\mathrm{effective}} \rangle}{V_{\mathrm{nominal}}}, \tag{6}$$

where ρ represents density, δ is the Dirac delta function, r is the scalar radius and i and j are atoms that belong to chemical species A and B, respectively. The angle brackets denote the ensemble averages. The RDF of slab-like geometries is corrected by the global/local density ratio C during normalisation, which is equivalent to the effective/nominal volume ratio. The nominal volume is the volume of the simulation box, and the effective volume is the actual volume occupied by the slab structure, which is calculated by the enclosed contact and re-entrant surfaces.[25]

The stages throughout the dehydration process are characterised by the composition ratio n, which is the molar ratio between water molecules and $MgSO_4$ ions in a local or global region. In case of global n value, the ratio is taken between the number of confined water molecules N_{conf} and the number of $MgSO_4$ ions $N_{\mathrm{MgSO_4}}$, which is a constant of 300 as mentioned earlier. Note that the initial global n value is 7.0, and $n = 0$ indicates complete dehydration.

To validate the energy terms in the simulation, normal mode analyses were used to correct the classical simulation results following harmonic approximation.[26] This method was well validated through the heat capacity calculation of a metal system.[27] The corrected

total energy can be obtained from

$$H_{QM} = H_{CL} + k_B T \sum_{i=1}^{3N-3} \left(\frac{1}{2} x_i - 1 + \frac{x_i}{e^{x_i} - 1} \right), \qquad (7)$$

where H_{QM} and H_{CL} are quantum mechanical and classical enthalpies, $x_i = h\nu_i/k_B T$, and ν_i are vibration frequencies of normal modes calculated from the normal mode analyses. The summation is over all degrees of freedoms except for 3 coming from the centre of mass motion.

3. Results and discussions

3.1 *Dehydration process*

In the endothermic dehydration simulation, the total potential energy in the simulation box increased with time while the total number of water molecules decreased, as illustrated in Figure 2. In the early stage of dehydration (0–15 ns), a rapid evasion of surface layer water molecules was observed from the simulation, and the number of confined water molecules N_{conf} quickly dropped from an initial value of 2100 to around 1650. In around 15–25 ns, the dehydration slowed down, followed by a temporary reacceleration, before it eventually detained. The reacceleration could be the result of the Smith–Topley [28] effect, which stated that the water molecules adsorbed on the surfaces could serve as catalyst for dehydration. Further investigation is needed to support this statement. After 300 ns of simulation, the dehydration was not complete, and the composition ratio n was decreased to approximately 1.2 ($N_{conf} = 355$, Figure 3), compared with an experimental value of 0.8 from thermogravimetric analysis.[2]

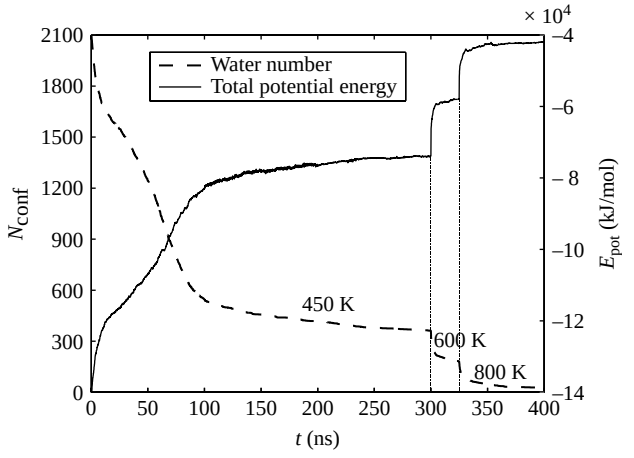

Figure 2. Number of confined water molecules N_{conf} and total potential energy E_{pot} in the simulation box as functions of simulation time. The simulation temperature is 450 K for the first 300 ns, 600 K for 300–325 ns, and 800 K for 325–400 ns.

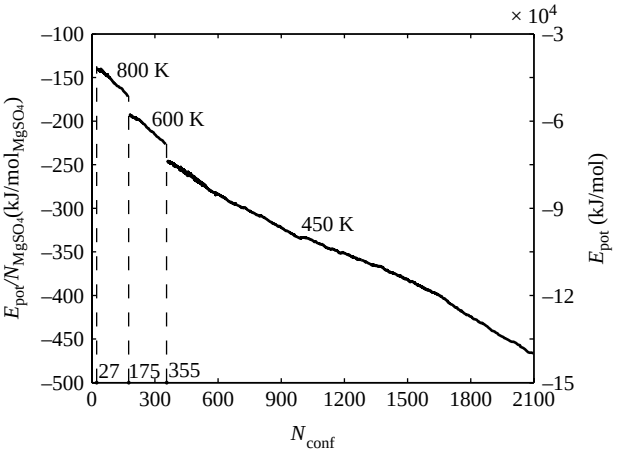

Figure 3. Total potential energy per mole of $MgSO_4$ as a function of the number of confined water molecules N_{conf}.

The total potential energy E_{pot} with respect to N_{conf} is plotted in Figure 3. The total potential energy jumps when temperature is increased. Assuming a linear dependence of potential energy on the water number, by linear regression of the 450 K curve, the slope is -36.34 ± 0.09 kJ/mol with a 95% confidence level. This value can be viewed as the average binding energy per water molecule into the crystal slab. Considering a complete dehydration process from $MgSO_4{\cdot}7H_2O$ to anhydrous $MgSO_4$, and taking the above average binding energy value, the total reaction enthalpy for complete dehydration is estimated to be 254.38 ± 13.50 kJ/mol, compared with an experimental value of 354.0 kJ/mol.[2] Note that the experimental result is measured using a differential scanning calorimetry heat flux technique during the heating up process, while the simulation is carried out at a constant temperature scheme. To further validate the simulation result, supplementary equilibrium MD simulations of bulk epsomite were carried out at 300 and 450 K. Both NpT simulations consisted of 64 epsomite molecules, in combination with periodic boundary conditions. After energy minimisation and equilibration, the ensemble averages of the classical enthalpies from the 500 ps trajectories (500 configurations) are calculated. It is worth mentioning that both NpT simulations lead to structurally stable systems. Then we took the resultant configurations for a thorough energy minimisation by a combined conjugate gradient and steepest descent method, before calculating the Hessian matrix for normal mode analyses. The corrected enthalpy difference according to Equation (7) between 300 and 450 K was then obtained to be 84.58 ± 3.22 kJ/mol. According to Hess's law, this adds up to 339.0 ± 13.9 kJ/mol of dehydration energy, close to the experimental value of 354.0 kJ/mol.

3.2 Partial densities

Partial densities of water and $MgSO_4$ components were calculated separately according to Equation (4). In the early dehydration stages, the local densities were less dependent on x and y coordinates. To study the local density changes in z-direction, local regions were defined as sliced bins stacked along z-direction, each 0.005 nm wide. Then the densities are averaged from 1000 configurations within 100 ps of simulation. The results are shown in Figure 4. Throughout the thermal dehydration process, several distinct density profiles can be recognised as representations of different dehydration stages. The numbering below is in accordance with that in Figure 4.

(a) At the initial stage, there are evident periodic peaks that indicate a crystalline structure. The average bulk density is 1560 kg/m^3, as compared with an experimental value of 1670 kg/m^3 at atmospheric temperature and pressure.

(b) The water near or on top of the crystal surface quickly evaded into the vacuum. Within 5 ns, one seventh of the water molecules were removed from the system, and in another 25 ns, another seventh of water molecules were removed. The partial density profiles show that the loss of water starts from the surface layer, forming a gradient in water number towards the centre. Under the attraction forces, the crystal began to shrink, and two peaks in the $MgSO_4$ partial density appeared. The periodic peaks of the crystalline structure are no longer evident under the rapid loss of water, which is possibly due to the collapse of the crystal framework and formation of amorphous phases. [7,8] However, a rough symmetry around the central plane is still existent.

(c) The two peaks in the $MgSO_4$ density grow higher and begin to move towards the centre. The thickness of the slab continues to decrease. The partial density of water near the centre approximately remains unchanged while the surface water partial density keeps decreasing.

(d) The peak of the water partial density near the centre is leveled off, accompanied with a slowdown of the dehydration rate. The two peaks in the $MgSO_4$ density have merged and become indistinguishable. In this stage, the thickness of the crystal slab is no longer uniform, and the slab surface is no longer flat. The superficial texture and the geometry of the slab are not symmetric about the central plane. The thinnest part of the slab approaches to zero, prior to the formation of hollow regions. Therefore, the

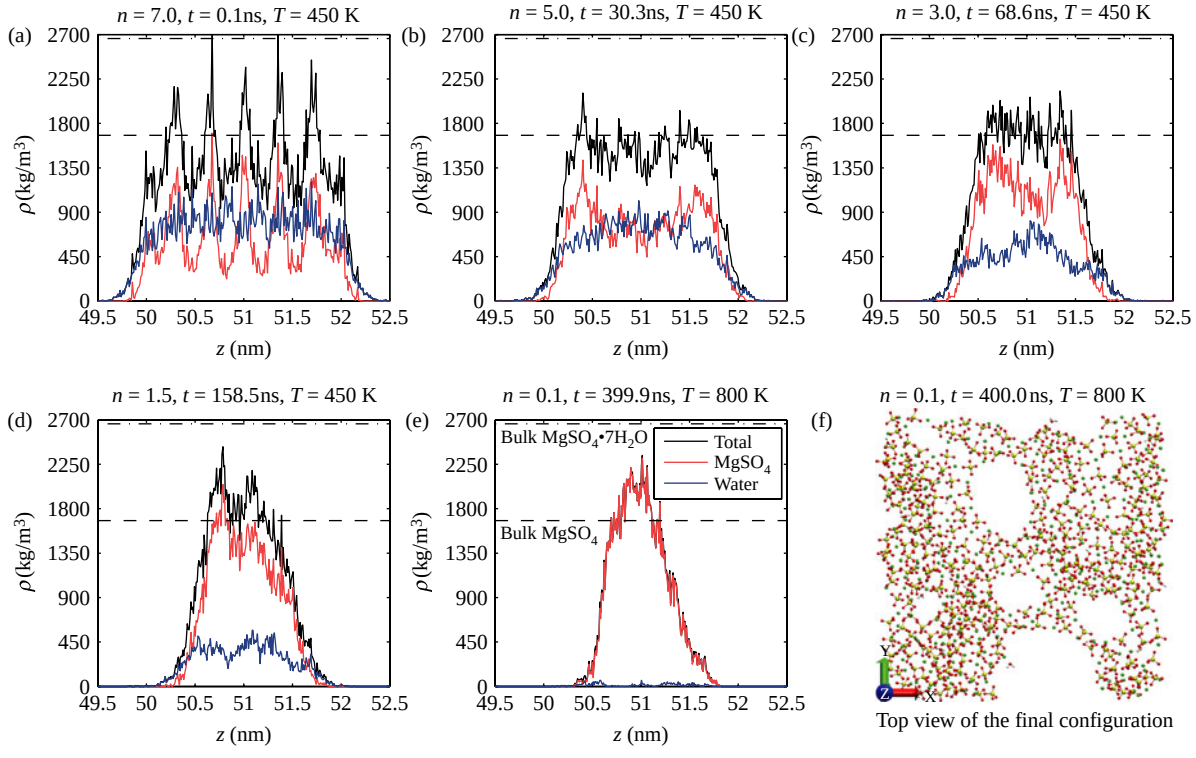

Figure 4. (Colour online) (a) to (e) Local partial densities of water (blue) and $MgSO_4$ (red) in z-direction as the composition ratio n changes from 7.0 to 0.1. The dashed lines are referenced bulk densities of $MgSO_4$ and $MgSO_4{\cdot}7H_2O$) at ambient conditions. (f) Top view snapshot taken at $t = 400$ ns at the end of the simulation.

partial density of water in the centre part shown in the figure is partly contributed by water adhered on the internal surfaces.

(e) The final density profile when the temperature was raised to 800 K does not reach that of bulk anhydrous $MgSO_4$, because of the hollow regions formed, probably because of surface tension. This is illustrated in the top view screenshot in Figure 4 (f). These hollow regions can also be identified as initial cracks from volume shrinkage in micro grain particles, which develop into a porous structure.

A further understanding of the slowdown of the dehydration rate ascribes to the analysis of local composition ratios shown in Figure 5. Although the dehydration process is characterised by the systems composition ratio n, the local ratios may differ from the average value. To give a general tendency of the ratio curve without loss of the details, Figure 5 presents both bin-wise ratios and trend lines which are fitted by fourth power polynomials, symmetric to the centre plane that passes through the systems mass centre. The higher local n values near the surfaces come from the adhered surface water molecules, where no $MgSO_4$ ions are present. In the centre part, local n values do not change much in the early stages of dehydration ($n = 7.0$, 5.0) and a gradient in n is formed. At later stages ($n = 3.0$, 1.5, 0.1), n in the centre region decreases and the gradient in the n profiles decreases accordingly.

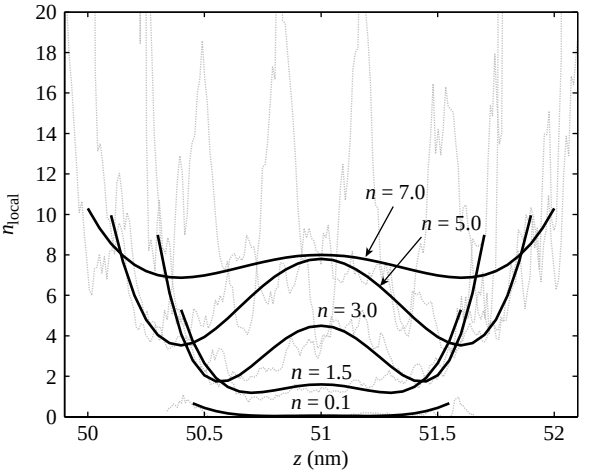

Figure 5. Local composition ratios n, local along z-direction at different dehydration stages in the simulation. The grey dashed lines are the bin-wise ratios and the thicker solid lines are trend lines fitted by fourth power polynomials symmetric to the centre plane.

3.3 *Radial distribution functions*

The structural changes throughout the dehydration are characterised by RDFs. To make a good comparison with simulated bulk crystals, the calculated RDFs of the slab structures are multiplied with factor C, as described in Equation (6), to ensure that the local densities are the averaged densities within the slab structures. In Figure 6, four sets of RDFs are plotted, with Mg, O_W, O_S, O, S and H representing magnesium dications, oxygen atoms in SPC water molecules, oxygen atoms in sulphate dianions, all oxygen atoms, sulphur atoms and hydrogen atoms, respectively. The RDFs of crystalline $MgSO_4{\cdot}7H_2O$ and $MgSO_4$ are represented by thick lines in Figure 6. These are calculated from equilibrium NpT MD simulations of bulk crystals at 450 K with initial configurations generated from neutron diffraction data.[20,29] The simulation for epsomite consisted of 180 molecules and for $MgSO_4$, 480 molecules. Both simulations lasted for 500 ps with 500 configurations sampled. The RDFs of the final configuration at 800 K and 400 ns when $n = 0.1$ are also plotted as a reference.

Accompanied with water loss, the RDF peaks change in both height and position. One evident shift is recognised in the second peak in Figure 6(c), which corresponds to the H···O hydrogen bonds. The increasing average H···O bond length is confirmed by DFT calculations.[12] The decrease in the first peak in Mg – O_W (Figure 6(b)) and the increase in the first peak in Mg–O_S (Figure 6(a)) support the loss of water and the clustering of magnesium and sulphate ions. This is also concluded from the density analysis as presented in the previous section.

Note that the discrepancies in RDFs calculated from bulk and slab simulations are expected, because the RDFs in the slab geometries will converge to the effective/nominal volume ratio C in Equation (6). This geometry effect underestimates the intensity of the peaks at larger r but keeps correct peak intensity at smaller r. The disagreement between the $n = 7.0$ curve with the crystalline epsomite (Figure 6(a–d)) curve comes from the geometry effect mentioned above on the one hand and from the surface rearrangement during energy minimisation and initial MD steps on the other hand. The RDF profiles in the final configuration differ from the RDF profiles of crystalline $MgSO_4$ (Figure 6(a),(d)), indicating that the newly formed anhydrous $MgSO_4$ possesses a disordered structure and therefore has a different RDF. Both van Essen et al. [2] and Ruiz-Agudo et al. [30] mentioned a recrystallisation process of the dehydrated amorphous precursor. However, this possibly slow reorganisation of the lattice structure was not observed in the simulation. It is not fully clear whether there are intermediate products (hexa-, tetra-, di- and mono-hydrate), as no sharp characteristic peaks are observed.

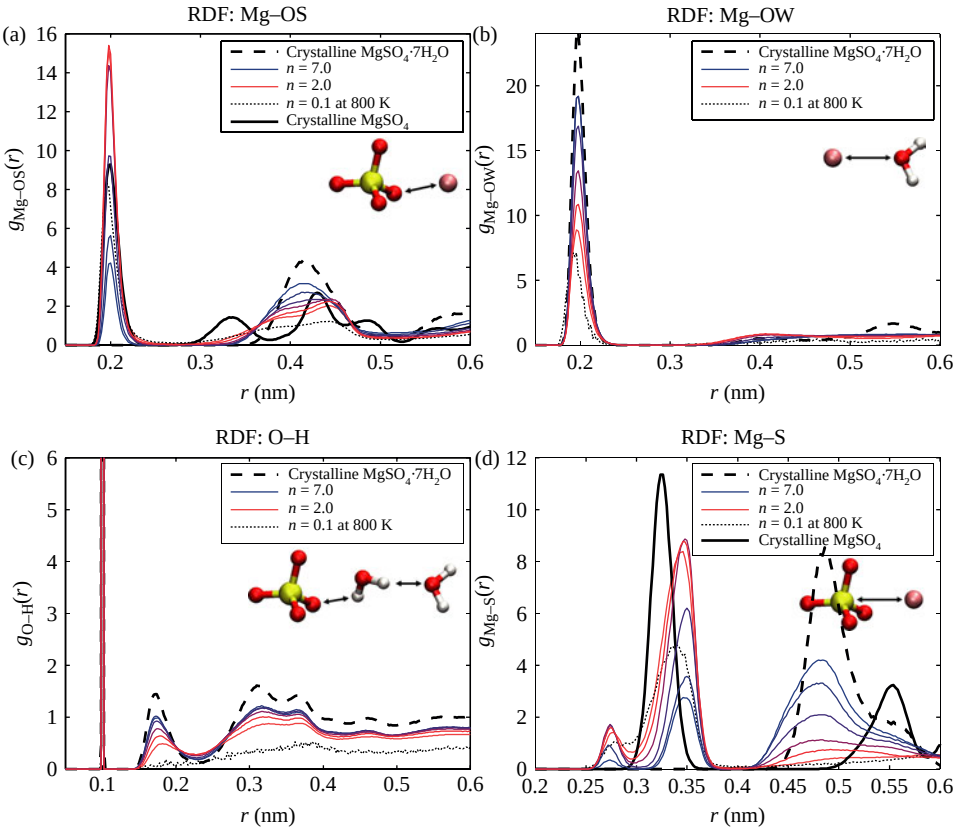

Figure 6. (Colour online) Calculated radial distribution functions (RDFs) of (a) Mg – O_S; (b) Mg – O_W; (c) O – H; (d) Mg – S. The thick lines are the RDFs predicted by bulk epsomite and $MgSO_4$ simulations, as comparisons. The changing colour lines from blue to red represent mean composition ratio n of 7.0, 6.0, 5.0, 4.0, 3.0, 2.0. The thin dotted lines are the RDFs of the final configuration at 800 K.

3.4 Mass diffusion of water

Based on the density analyses, after the quick removal of surface water molecules, the dehydration process is governed by the slow diffusion of water from the inner layers to the surface. Compared with water, the $MgSO_4$ ions are less mobile and act as the framework of the structure. Therefore, we quantify the mass transfer in the dehydration process by the local diffusion coefficient of water molecules.

To obtain good ensemble averages, trajectories of 100 ps length are selected in the calculations. Local regions are defined by slicing the slab into many pieces, analogous to the density calculations. The bin widths are chosen to be 0.50 nm, larger than the mean free path of liquid water. Note that the data points are only 0.10 nm apart but represent the diffusion coefficients in a 0.50-nm wide region. In this way, the particles that are oscillating around a bin surface will be included in the calculation of the adjacent bin. Whether a water molecule is counted into the diffusion calculation of a certain region is determined by its duration of stay in this region. The choice of the minimum duration of stay t_m below which the molecule is not counted depends on the specific system of interest. Shinoda et al. [31] argued that the diffusion coefficient of water was not sensitive to the choice of duration in the range of 2–10 ps in lipid bilayer systems. Meanwhile, Taylor et al. [32] selected 2 ps in his study of nanometer water films. In this study, the diffusion coefficients in centre regions are not influenced by the choice of t_m, as the water molecules are trapped in the crystal for a longer timescale. However, near surface regions, they can be affected, because of the fast evasion movement of surface water molecules into the vacuum space. To determine the optimal t_m in the diffusion coefficient calculation, we compared different MSD curves in a local region near the surface. This is illustrated in Figure 7. We tested the cases when t_m equals to 5, 3 and 2 ps. Only the molecules that stay longer than t_m are included in the MSD calculation. The trajectories of these molecules are divided into segments of length t_m and are considered as molecules that have newly entered the local region. For instance, suppose a water molecule enters the local region at the 7th picoseconds and exits at the 12th picoseconds of the selected 100 ps long trajectory. We define t_0 as the moment at which a water molecule enters the local region. With $t_m = 2$ ps, its moving path will be divided into three segments: 7–9, 9–11 and 11–12 ps. Then the first two

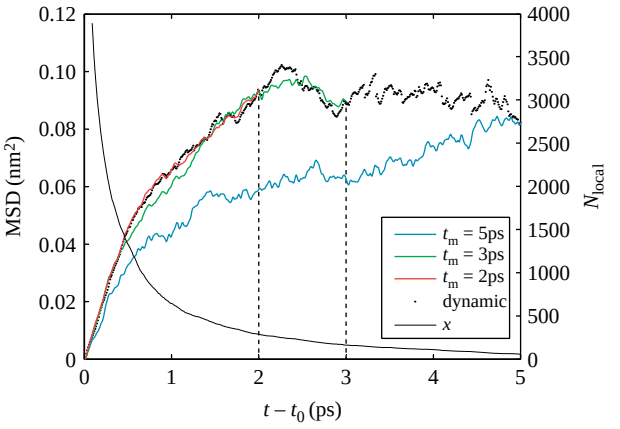

Figure 7. (Colour online) Mean square displacements (MSDs) of water molecules within a local region near the solid slab surface by different molecule selection criteria (minimum duration of stay t_m) and the number of water molecules N_{local} that stays in the local region for a period of time greater than $(t - t_0)$, where t_0 is the moment a water molecule enters the local region. Black dots labels a dynamic averaging scheme counting all molecules that are present at time $(t - t_0)$.

segments are included in the MSD calculation as two independent molecules with $t_0 = 7$ ps and $t_0 = 9$ ps, and the third segment is discarded. In case of the dynamically averaged MSD (Figure 7, black dots), the mean value is taken over all molecules that are present at time $(t-t_0)$ without segmentation. Note that N_{local}, the number of water molecules that stay in the local region longer than $(t-t_0)$, decays with $(t-t_0)$ significantly. After about 2.3 ps, the dynamically averaged MSD stops increasing, as the slower molecules then come into play. Since any choice for the value of t_m will exclude a number of molecules that stays less than t_m into the MSD calculation, the question to be addressed now is till what t_m, will the selected molecules best represent the excluded ones (t_m as short as possible), while at the same time, the trajectory segments are still long enough to ensure a reliable linear fit. From Figure 7, it can be seen that $t_m = 5$ ps or 3 ps are not good choices. The linear fit of these two curves (0.8–5 and 0.8–3 ps) gives lower diffusion constants than that from $t_m = 2$ ps (fitted from 0.8 to 2 ps). This is because the selected molecules that stay longer than 5 ps or 3 ps are much slower and cannot represent those excluded faster molecules. However, the choice of $t_m = 2$ ps is reasonably better, as its curve has a good agreement with the dynamically averaged MSD plots. Therefore, we identify 2 ps as a proper choice of t_m to best preserve the diffusion properties without underestimation of the diffusion coefficients. We sorted out all water molecules that stayed longer than 2 ps in the selected trajectories, and divided the trajectories of individual water molecules according to the aforementioned segmentation rule. The diffusion coefficients are then calculated by fitting the linear region in the MSD curve from 0.8 to 2.0 ps.

In Figure 8, the 3D and directional diffusion coefficients of water D_{xyz} and D_z are plotted as functions of the z-coordinate for several global n values. Both D_{xyz} and D_z are higher at surface regions regardless of n, as illustrated in Figure 8. In the centre region, both D_{xyz} and D_z are less dependent of the z-coordinate. Also, D_{xyz} and D_z seem to increase with decreasing n. However, this could be partially contributed by the uneven slab surfaces that locate near centre regions, given that the diffusion coefficients are higher at the surface regions. The diffusion coefficients in the centre are in the order of 10^{-10} m^2/s, while those near surface are in the order of

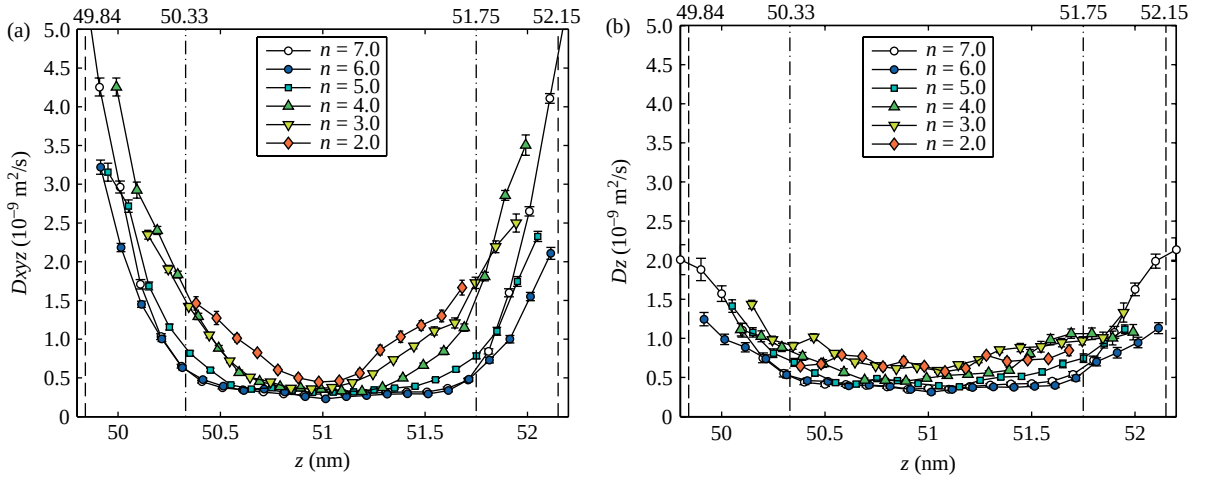

Figure 8. (Colour online) (a) Local diffusion coefficients D_{xyz} and (b) z components of local diffusion coefficients D_z, within the solid slab at various dehydration stages. The error bars represent the standard deviations of linear regression. The dashed and dash-dot lines label the coordinates of the slab surfaces at $n = 7.0$ and $n = 2.0$. The surfaces are defined by the locations where the density is 20% of the averaged bulk densities.

10^{-9} m^2/s. This falls into the same order of magnitude of a very recent research on the dehydration of $MgCl_2 \cdot 6H_2O$ at the same temperature, which gives values ranging from 8.5×10^{-10} to 3.7×10^{-9} m^2/s.[33] For comparison, the diffusion coefficient of saturated SPC liquid water at the same temperature (450 K, 890.35 kg/m^3) is also computed to be $18.9 \pm 0.6 \times 10^{-9}$ m^2/s in the same order of magnitude but higher than that of the water molecules on the slab surfaces. This may lead to discussions on the role of the presence of $MgSO_4$ ions. The higher diffusion rates of the surfaces come from the breakdown of the hydrogen-bonding network [32] and the collapse of the lattice frameworks.[7,8] The slow diffusion kinetics in the centre region seems to limit the dehydration rate and, therefore, the dehydration process can be characterised as a diffusion-driven process. In the $n = 2.0$ plot in Figure 8(b), D_z is no longer evidently larger in the surface regions but approximately shows a constant value. This indicates that the diffusion in z-direction has almost reached a steady state, and further dehydration is more difficult.

Another aspect of the mass diffusion of water is its anisotropic behaviour. This is most evident on the surface regions where D_{xyz} values are much larger than D_z values. The water molecules have more mobility along the surface than perpendicular to the surface. This conclusion suggests that the internal porous structure and the surface/volume ratio are crucial to the vapour transport by diffusion in the dehydration process.

4. Conclusions

MD simulations have been applied to investigate the thermodynamic and diffusion properties as well as structural changes during the thermal dehydration of a cleaved epsomite ($MgSO_4 \cdot 7H_2O$) crystal. In this study, the enthalpy change during dehydration and the bulk densities are calculated and compared with experimental values that validated the method. It is discovered that the dehydration process exhibits multiple stages. The initial quick dissociation and loss of surface water caused the high initial dehydration rate, accompanied by the collapse of the crystal framework and formation of amorphous phases. Following the loss of surface water, a density gradient of water is formed and the partial density of $MgSO_4$ is raised near the two surfaces. Subsequently, the rate of dehydration is seemingly controlled by the diffusion of water from the centre part to the slab surfaces. Eventually, the surface adsorption of water further inhibited the diffusion of water to the surfaces, and the diffusion in z-direction gradually reaches the steady state. The exothermic adsorption process can be reduced by increasing the simulation temperature. Superficial texture changes were observed during the simulation and evolved into hollow regions due to the volume shrinkage. It is also noted that the diffusion of water is anisotropic, suggesting that the internal porous matrix structures in the porous epsomite reactant play an important role in the water transport. Recrystallisation is not observed in this simulation owing to the slow lattice reorganising kinetics. The results obtained in this study agreed with corresponding experiments, and led to more insight into the thermal dehydration process of epsomite.

Acknowledgement

The research leading to these results has received funding from the European Community's Seventh Framework Programme (FP7/2007–2013) under grant agreement 296006. This work was also supported by Erasmus Mundus SELECT program.

References

[1] N'Tsoukpoe KE, Liu H, Pierrs NL, Luo L. A review on long-term sorption solar energy storage. Renewable Sustainable Energy Rev. 2009;13:2385–2396.
[2] van Essen VM, Zondag HA, Gores JC, Bleijendaal LPJ, Bakker M, Schuitema R, van Helden WGJ, He Z, Rindt CM. Characterization of $MgSO_4$ hydrate for thermochemical seasonal heat storage. J Sol Energy Eng. 2009;131:041014-1–041014-7.
[3] Hongois S, Kuznik F, Stevens P, Roux JJ. Development and characterisation of a new $MgSO_4$-zeolite composite for long-term thermal energy storage. Sol Energy Mater Sol Cells. 2011;95:1831–1837.
[4] Galwey AK, Brown ME, editors. Thermal dehydration of hydrated salts. Thermal decomposition of ionic solids, Chapter 7; 1999 p. 217–268.
[5] Ford RW, Frost GB. The low pressure dehydration of magnesium sulphate heptahydrate and cobaltous chloride hexahydrate. Can J Chem. 1956;34:591–599.
[6] Lallemant M, Watelle-Marion G. Dégradation thermique du sulfate de magnésium heptahydraté sous pression de vapeur deau contrôlée. Mécanisme observé au-dessus de 50 torr. Comptes rendus des séances de l'Académie des sciences, Paris, Série C. 1967;264:2030–2033.
[7] Wang A, Freeman JJ, Jolliff BL, Chou I. Sulfates on Mars: a systematic Raman spectroscopic study of hydration states of magnesium sulfates. Geochimica et cosmochimica acta. 2006;70:6118–6135.
[8] Brotton SJ, Kaiser RI. *In situ* Raman spectroscopic study of gypsum ($CaSO_4 \cdot 2H_2O$) and epsomite ($MgSO_4 \cdot 7H_2O$) dehydration utilizing an ultrasonic levitator. J Phys Chem Lett. 2013;4:669–673.
[9] Chipera SJ, Vaniman DT. Experimental stability of magnesium sulfate hydrates that may be present on Mars. Geochimica et cosmochimica acta. 2007;71:241–250.
[10] Wang A, Freeman JJ, Jolliff L. Phase transition pathways of the hydrates of magnesium sulfate in the temperature range 50°C to 5°C: implication for sulfates on Mars. J Geophys Res Planets. 2009;114: E04010-1–E04010-28.
[11] Iype E, Hütter M, Jansen APJ, Nedea SV, Rindt CCM. Parameterization of a reactive force field using a Monte Carlo algorithm. J Comput Chem. 2013;34:1143–1154.
[12] Iype E, Nedea SV, Rindt CCM, van Steenhoven AA, Zondag HA, Jansen APJ. DFT study on characterization of hydrogen bonds in the hydrates of $MgSO_4$. J Phys Chem C. 2012;116:18584–18590.
[13] Zhang WJ, Huo CF, Feng G, Li YW, Wang J, Jiao H. Dehydration of goethite to hematite from molecular dynamics simulation. J Mol Struct THEOCHEM. 2010;950:20–26.
[14] Krokidis X, Raybaud P, Gobichon AE, Rebours B, Euzen P, Toulhoat H. Theoretical study of the dehydration process of boehmite to γ-alumina. J Phys Chem B. 2001;105:5121–5130.
[15] Groot SRde, Mazur P. Non-equilibrium thermodynamics. Amsterdam: North-Holland Pub. Co.; 1962.

[16] Oostenbrink C, Villa A, Mark AE, Van Gunsteren WF. A biomolecular force field based on the free enthalpy of hydration and solvation: the GROMOS force-field parameter sets 53A5 and 53A6. J Comput Chem. 2004;25:1656–1676.
[17] Berendsen HJC, Postma JPM, van Gunsteren WF, Hermans J. Interaction models for water in relation to protein hydration. Intermol Forces. 1981;11:331–342.
[18] Sakamaki R, Sum AK, Narumi T, Yasuoka K. Molecular dynamics simulations of vapor/liquid coexistence using the nonpolarizable water models. J Chem Phys. 2011;134:124708.
[19] Darden T, York D, Pedersen L. Particle mesh Ewald: an N log(N) method for Ewald sums in large systems. J Chem Phys. 1993;98:10089.
[20] Fortes AD, Alfredsson M, Vočadlo L, Knight KS. The thermoelastic properties of $MgSO_4 \cdot 7D_2O$ (epsomite) from powder neutron diffraction and *ab initio* calculation. Eur J Mineral. 2006;18:449–462.
[21] Berendsen HJ, Postma JPM, van Gunsteren WF, DiNola A, Haak J. Molecular dynamics with coupling to an external bath. J Chem Phys. 1984;81:3684–3690.
[22] Hess B, Kutzner C, Pvan der Spoel D, Lindahl E. GROMACS 4: algorithms for highly efficient, load-balanced, and scalable molecular simulation. J Chem Theory Comput. 2008;4:435–447.
[23] Sugii T, Takagi S, Matsumoto Y. A molecular-dynamics study of lipid bilayers: effects of the hydrocarbon chain length on permeability. J Chem Phys. 2005;123:184714.
[24] Allen MP, Tildesley DJ. Computer simulation of liquids. New York: Oxford University Press; 1989.
[25] Richards FM. Areas, volumes, packing, and protein structure. Ann Rev Biophys Bioeng. 1977;6:151–176 PMID: 326146.
[26] McQuarrie DA. Statistical mechanics. New York: Harper & Row; 1976.
[27] Tojo T, Kawaji H, Atake T. Molecular dynamics study on lattice vibration and heat capacity of yttria-stabilized zirconia. Solid State Ionics. 1999;118:349–353.
[28] Topley B, Smith M. Function of water vapour in the dissociation of a salt hydrate. Nature. 1931;128:302.
[29] Fortes AD, Wood IG, Vočadlo L, Brand HEA. Crystal structures and thermal expansion of -$MgSO_4$ and -$MgSO_4$ from 4.2 to 300 K by neutron powder diffraction. J Appl Crystallogra. 2007;40:761–770.
[30] Ruiz-Agudo E, Martín-Ramos JD, Rodriguez-Navarro C. Mechanism and kinetics of dehydration of epsomite crystals formed in the presence of organic additives. J Phys Chem B. 2007;111:41–52.
[31] Shinoda W, Mikami M, Baba T, Hato M. Molecular dynamics study on the effects of chain branching on the physical properties of lipid bilayers: 2. Permeability. J Phys Chem B. 2004;108:9346–9356.
[32] Taylor RS, Dang LX, Garrett BC. Molecular dynamics simulations of the liquid/vapor interface of SPC/E water. J Phys Chem. 1996;100:11720–11725.
[33] Smeets B. Computer simulation on the dehydration and hydrolysis reactions of magnesium chloride hydrates [Master's thesis]. Eindhoven University of Technology; 2013.